Nitrogen Doped Graphene-Core/shell CdS@TiO₂ for Direct Electrochemistry of Hemoglobin and Hydrogen Peroxide Biosensor Application

En-yong Shi [1], Yu She [1], Ji-ping Yao [1], Xiao-jian Zou [3], Chuan-yin Liu[1, 2, 3]*

[1] School of Food S&T and Chemical Engineering, Hubei University of Arts and Science, Xiangyang 441053 P.R. China
[2] Hubei Key Laboratory of Low Dimensional Opto-electric Materials and Devices, Xiangyang 441053 P.R. China
[3] Drug testing laboratory, Public Security Bureau of Xiangyang, Xiangyang, 441000, P.R. China
[*]E-mail: liucyin2002@sina.com

Core-shell CdS@TiO₂ nanoparticles were synthesized and characterized by SEM, EDS. The as-prepared core-shell nanoparticles and nitrogen doped graphene were utilized to promote the electron transfer of hemoglobin. It is found that the nano-materials can effectively enhance the direct electron transfer of hemoglobin with symmetrical peak separation of 50 mV and formal peak potential of -0.395 V, and it is also found the formal potential shifts with pH in the range of 4.0-9.0 with a slope of 32 mV/pH to reveal a redox Bohr effect in the electron transfer process. The direct electron transfer (DET) of hemoglobin can also be estimated by heterogeneous electron transfer coefficient of 3.60 s^{-1}. The proposed biosensor shows its favourable reproducibility, stability and low detection limit (5.4×10^{-8} mol/L) for hydrogen peroxide and Michealis-Menten constant of 0.012 mmol/L.

Keywords: Core/shell CdS@TiO₂, hemoglobin, direct electrochemistry, hydrogen peroxide biosensor

1. INTRODUCTION

It is vital important to understand the mechanism of bio-logical redox reactions and selective electro-catalysis of enzyme-promoted biochemical reactions. In the practical experimental and theoretical research, the most commonly used method is to fabricate biosensor on solid electrodes to simulate the micro-environment of native redox proteins in human body and perform efficient electron transfer between redox proteins and electrode surface by adding some promoting reagents or materials to fabricate simulating layers. However, due to the deeply-enwrapped in the polypeptide chains, the

electro-active centers of proteins can hardly access to electrode surface to accomplish direct electron transfer. It is well-known that the peculiar conformation of proteins is the basement of carrying out its special bio-function, once the conformation of proteins changes, some of the special function may be hindered or weakened. Unfortunately, due to the easy to denaturation of enzyme and the difficult to opening its electroactive centre to achieve direct electron transfer toward electrode, and also the adsorption of enzyme onto the solid electrodes, it is very difficult to achieve direct electron transfer on bare solid electrodes [1]. To solve this problem, various methodologies have been utilized to fabricate electro-stimulating layers or to entrap redox enzyme into biocompatible films. In the recent years, considerable research have been focused on promoting electron transfer of redox proteins by using biocompatible film and nano-materials or meso-porous materials, such as carbon nanotubes[2], graphene[3] and nanoparticles[4], metal and oxide nanoparticles[5], nano-materials composite[6-8], and so on.

Core–shell nanostructure is a kind of assembled structure in proper order, which is composed of a kind of nano-materials as core and another type of nanomaterials as a wrappage via chemical bonds or other interactions, has attracted researcher's attention in many fields including biomedical and optical applications, bioelectronics and biocatalyst [9-10]. It can display many new characters that single nanoparticles do not own and has much broader prospects in practical and theoretical application than the single ones. The core@shell structure has some advantages as compared to single nanomaterial: Firstly, it could hold back the intrinsic nanomaterials suffering from chemical or physical changes due to the existence of relatively stable shell; Secondly, the outer shell can not only effectively enhance the conductivity, activity, stability and difference of the core nanomaterial, but also give the core materials with some peculiar features as electromagnetic, optical and electro-catalytic properties. When core@shell nanomaterials were used to adsorb or immobilize enzymes, the electron transfer activity and bio-catalytic performance of enzymes would be improved correspondingly [11-12]. Within the research field of the third-generation biosensors, it is found that the immobilization of biomolecules onto the electrode modified with different nanomaterials can effectively improve the reliable, sensitive, accurate and low-cost properties of biosensors. In recent years, different nanomaterials including core@shell nanomaterials have been utilized to fabricate biosensors by altering the synthetic procedure and material composition to enhance its electrocatalytic and bio-conductive ability. Meanwhile, the progress in the development of new biosensors based on the integration of biomolecules and core@shell nanomaterials requires advance of the materials and novelty of ways. Therefore, it is quite necessary to quest for an ideal nanomaterial and efficient method to develop the enzyme-based biosensors. Carbon nano-materials, such as CNTs, graphene, carbon nano-particles have been used for stimulated layer [2-3, 7-8], and some core/shell nano-structure has been used to entrap enzyme or proteins to fabricate biosensors, such as Ag@C [10], CdSe@CdS quantum dots [11], $Fe_3O_4@Pt$ [13], Au@Ag nanorods[14] and $Fe_3O_4@C$–Au nanocompo-site [15], $Fe_3O_4@Al_2O_3$ [16], $Fe_3O_4@Au$ [17] and core-shell heme protein-Au-polydopamine-Fe_3O_4 magnetic bionano-particles [18].

In the present work, the nitrogen doped grapheme (NGR) and core@shell $CdS@TiO_2$ was prepared respectively, and the as-prepared nano-materials were used to immobilize hemoglobin for the fabrication of hydrogen peroxide biosensor. The direct electrochemistry of hemoglobin was

investigated and the electrocatalysis was evaluated with fast electron transfer rate and low Michealis-Menten constant.

2. EXPERTIMENTAL

2.1 Reagents and apparatus

Cd(NO$_3$)$_2$, Na$_2$S, H$_2$O$_2$ (30%), butyl titanate and other chemicals were purchased from Shanghai Chemicals Corp. (Shanghai, China). Nitrogen doped graphene (NGR) was synthesized according to the reference [19] with minor modifications. Briefly, the prepared graphene oxide was sonicated and dispersed for 1h in pure water to keep its concentration of 2mg/mL. Then the dispersed solution was centrifugally separated for 5min at 1000rpm to remove the unresolved GO residues. The as-prepared GO solution was adjusted to pH 10 with 30% aqueous ammonia, and 2mL hydrazine hydrate was added and magnetically stirred for 10 min and then the mixed solution was transferred into a Teflon autoclave to react for another 3h at 80°C with microwave. The synthesized NGR was magnetically stirred, washed, and vacuum dried at 50°C. The prepared material was characterized by SEM and FTIR. Seen from the figures of NGR, the sheets of NGR fold together and frizzle on the edge of NGR; this is the traditional feature of graphene. Comparing with the FTIR spectra of graphite oxide and NGR, the spectra is much simple for NGR, indicating that during the chemical reaction of hydrazine hydrate with graphite oxide, most of the groups containing oxygen have been removed and constructed graphene containing doped nitrogen, and the 1565cm^{-1} absorption peak conferred the existence of C=C bond [19]. 0.1 mol/L Phosphate buffer solution (PBS) with different pH value was prepared with Na$_2$HPO$_4$ and KH$_2$PO$_4$, and adjusted to a suitable value with 0.2 mol/L NaOH.

The electrochemical experiments were performed in a CHI 660E electrochemical workstation (USA) with traditional three electrode cell, which was composed of bare Au and modified Au electrode as working electrode, saturated Ag/AgCl as reference electrode and Pt wire as the counter electrode. The synthesis of CdS@TiO$_2$ was performed with ultra-sonic mixing and hydrothermal methods. The characterization of CdS@TiO$_2$ was accomplished with scanning electric microscopy (SEM) and energy dispersive spectrometer (EDS) (S-4800, Japan). UV-Vis spectra were obtained from UV spectrometer (UV-1800, Shimadzu, Japan).

2.2 Synthetic procedure of CdS@TiO$_2$ and preparation of modified electrodes

0.1 mol/L CdSO$_4$ and Na$_2$S were prepared and mixed in a round-bottom flask by electro-magnetic mixing for 8 hours under 160°C, then the yellow product was centrifugally separated and washed with pure water and ethanol for three times, respectively. The as-prepared CdS was vacuum dried at 60°C for 30 hours. 10 mg CdS was sonciated-solved in 50 mL ethanol (95% purity), then 50 mL ethanol solution containing 2 mL triethanolamine, 0.5 mL acetic acid and 0.64 mL butyl titanate was added to CdS turbid liquid to react 3 hours under sonication and ageing for 8 hours, the product was centrifugal separated and vacuum dried for 5 hours at 60°C.

The bare Au electrode was polished mirror-finish and firstly modified with 15 μL NGR-THF solution (2 mg/mL), after the NGR modified electrode was dry, then 15 μL CdS@TiO$_2$+Hb mixture was further modified onto the NGR modified Au electrode surface (named as NGR-CdS@TiO$_2$-Hb/Au) (content of CdS@TiO$_2$ and Hb in the mixture were 4 mg/mL and 5 mg/mL, respectively). The Au electrode modified with TiO$_2$-Hb, NGR-Hb and CdS@TiO$_2$-Hb, was named as TiO$_2$-Hb/Au, NGR-Hb/Au and CdS@TiO$_2$-Hb/Au, respectively.

2.3. Electrochemical characterization and investigations

In 0.1 mol/L KCl containing 1 mmol/L Fe(CN)$_6^{3-/4-}$, cyclic voltammetry and electrochemical impedance spectroscopy were accomplished for bare Au and modified Au electrodes. In deoxygenated PBS with suitable pH value, the proposed modified Au electrode was used as working electrode, cyclic voltammetry and amperometric i-t curves were used to evaluate the electrochemical behaviours of direct electron transfer and electrocatalysis towards hydrogen peroxide.

3. RESULTS AND DISCUSSION

3.1 Characterization of CdS@TiO$_2$

The SEM and EDS figures of core/shell CdS@TiO$_2$ nano-particles were shown in Fig.1. As can be seen, the CdS nanoparticles with average diameter of 20-30 nm, and the core/shell CdS@TiO$_2$ nanoparticles with average diameter of 30-40 nm can be observed in the SEM figure. Further EDS investigation of the core/shell nanoparticles, from the content of the elements, it can be found that Cd and S are almost similar content, (Cd 17.34% and S 16.52%), while the Ti content is much smaller, only 3.30% and O 62.84%, indicating that the shell is thin over the CdS core, the result also verifies the SEM figure, the diameter of CdS@TiO$_2$ is a little larger than that of CdS. This result indicates that TiO$_2$ has been composed as a shell on the CdS nanoparticles.

The Soret band of protein UV–vis spectrometry is sensitive to the variation of the micro-environment around the heme group and can provide information about the conformational integrity of the proteins [20]. Based on the UV-Vis experimental results, the Soret absorption of the native Hb, NGR-Hb, CdS@TiO$_2$-Hb and TiO$_2$-Hb is located at almost the same wavelength (about 407 nm). The native Hb has a soret absorption peak at 407 nm, however, the soret absorption peak for Hb-TiO$_2$ at 407 nm, a little shift of NGR-Hb at 405nm and CdS@TiO$_2$-Hb at 405 nm, respectively. All those results suggest that the natural structure of Hb has been maintained and the core/shell nanoparticles can be used as an effective modifier of Hb and can effectively maintain the bioactivity of Hb.
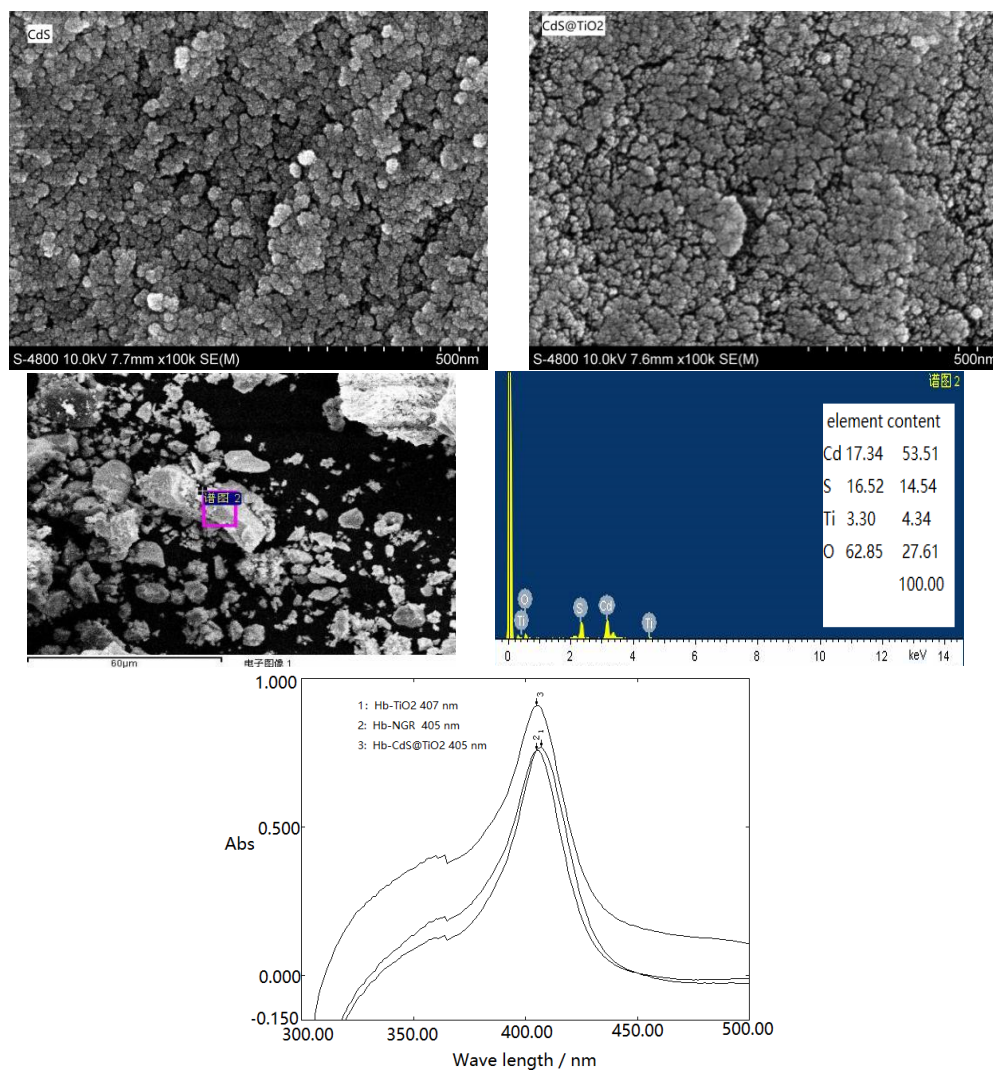
Figure 1. SEM figures of CdS & CdS@TiO$_2$ nanoparticles and EDS of CdS@TiO$_2$; UV-Vis spectra of Hb-TiO$_2$, Hb-NGR and Hb-CdS@TiO$_2$

3.2 Electrochemical characterization of different electrodes

Cyclic voltammetry and electrochemical impedance spectroscopy are the effective tools to characterize the modification of electrodes. Fig.2 is the Nyquist plots of bare Au, NGR-Hb/Au and CdS@TiO$_2$-Hb/Au in 0.1 mol/L KCl containing 1 mmol/L Fe(CN)$_6^{3-/4-}$. As can be seen, bare Au has a very little semi-circle in high frequency and a line about 45^0 in low frequency, which indicating that there is no substance to block the charge transfer of probe ions to arrive at the electrode surface. However, when the Au electrode was modified with NGR-Hb and NGR-CdS@TiO$_2$-Hb, it is obvious that the semi-circle of Nyquist plot increases, and the results maybe the further modification of Hb film which hinder the charge transfer of probe ions to achieve the electrode surface, however the hindrance effect is not strong, so the semi-circle increase a lot. For the cyclic voltammograms of bare Au, NGR-Hb/Au and NGR-CdS@SiO$_2$-Hb in 0.1 mol/L KCl containing 1 mmol/L Fe(CN)$_6^{3-/4-}$, the redox peak separation is only 65 mV at bare Au, but the peak separation increase to 100 mV and 124 mV at NGR-

Hb/Au and NGR-CdS@TiO$_2$-Hb/Au, respectively. All the impedance results are consistent to the cyclic voltammetric results.
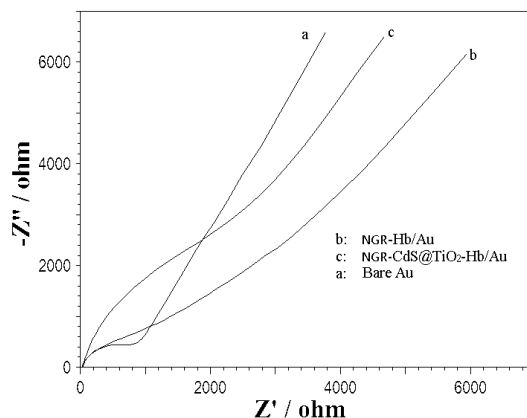

Figure 2. Nyquist plots of bare Au, NGR-Hb/Au and NGR-CdS@TiO$_2$-Hb/Au in 0.1 mol/L KCl containing 1 mmol/L Fe(CN)$_6^{3-/4-}$, applied potential: 0.24 V

3.3 Direct electron transfer of Hb in NGR-CdS@TiO$_2$ film

Fig.3 is the cyclic voltammograms of Hb at TiO$_2$-Hb/Au, NGR-Hb/Au, CdS@TiO$_2$-Hb/Au and NGR-CdS@TiO$_2$-Hb/Au in pH 7 PBS. It is known that most redox proteins exhibit low electron transfer rate on conventional electrode due to their embedded prosthetic groups and instability of the biological matrix at electrode surface [21]. In order to enhance the electrochemical activity and stability, biocompatible film and nano-materials have been utilized. So in later experiments, the cyclic voltammetric responses of Hb entrapped in TiO$_2$ sol, NGR, CdS@TiO$_2$ and CdS@TiO$_2$-NGR were investigated respectively. As can be seen from curve c, only a pair of weak redox response with large peak separation (about 300 mV) and weak currents can be observed, which suggested that the CdS@TiO$_2$ could merely support Hb into effective orientation for electron transfer. The cyclic voltammograms are stable and reproducible, which indicating that the single CdS@TiO$_2$ nanoparticles cannot be solely used for the DET investigation, but the core/shell nanoparticles can effectively maintain the bioactivity of Hb and decrease the passivation of Hb upon the Au electrode. On the contrary, when the Au electrode was modified with NGR-Hb, a pair of redox peaks at -0.38 V and -0.58 V can be seen from curve B, this pair of peaks are obvious accordance to the direct electron transfer of Hb. However, this pair of peaks will gradually decrease with the increase of scans, which indicates that the NGR can effectively promote the DET of Hb, but the persistence of bioactivity of Hb is inferior. However, upon addition CdS@TiO$_2$ into the modification of Au, a pair of well-defined and reproducible redox peaks was observed at the NGR-CdS@TiO$_2$-Hb/Au (curve A), indicating NGR and CdS@TiO$_2$ composite film can effectively enhance the direct electron transfer of Hb in the electrode surface. This pair of redox peaks appeared at -0.37 V and -0.42 V, with peak separation of 50 mV and formal potential of -0.395 V, the currents are ten times than that of NGR-Hb/Au. Obviously, the couple is attributed to the reversible redox process of the heme groups of native Hb [2,6,13,18]. Thus, it is suggested that the NGR-CdS@TiO$_2$ composite film could provide a favorable micro-environment

for Hb to maintain its biological activity and play an important role in promoting the direct electron transfer of Hb on the electrode surface.
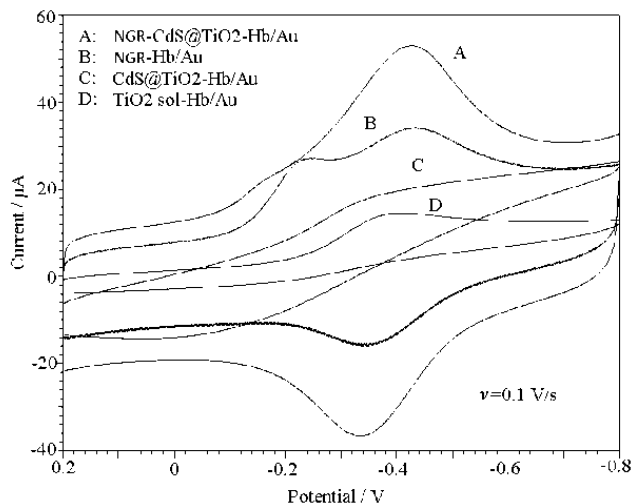

Figure 3. Cyclic voltammograms of TiO$_2$-Hb/Au (D), NGR-Hb/Au (B), CdS-TiO$_2$-Hb/Au (C) and NGR-CdS@TiO$_2$-Hb/Au (A) in deoxygenated pH 7 PBS.
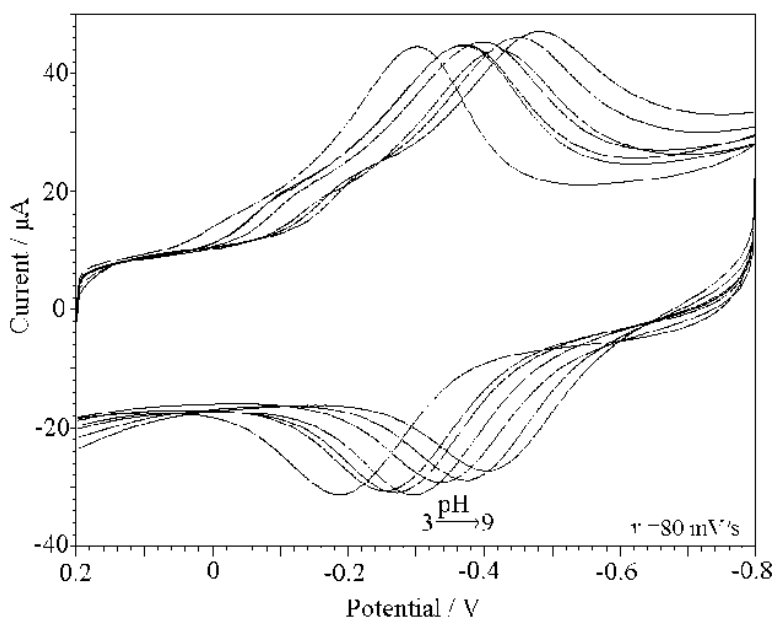
3.4 Effect of pH of electrolyte

Figure 4. Cyclic voltammograms of NGR-CdS@TiO$_2$-Hb/Au in different pH PBS.

pH value of electrolyte can affect the electrochemical behavior of electroactive substance on the surface of electrode. In the DET investigation, pH value can not only affect the DET behavior of redox protein, but also affect the proton state of redox protein [21]. In this experiment, different electrolytes such as KCl, NaAc-HAc, PBS and BR have been utilized; it is found that the electrochemical behavior of Hb is more symmetrical and strong in PBS. So in the latter experiment,

PBS has been selected as optimum electrolyte. For different pH value of PBS, the DET response of Hb entrapped in NGR-CdS@TiO$_2$ film has been studied, the results was shown in Fig.4. As can be seen, from pH 3 to 9, the symmetrical DET can be observed with peak potentials shifting negatively, and the peak potential is linear to pH with regressive equation of E_{pa}=-0.229-0.028pH, r=1 and E_{pc}=-0.0915-0.035pH, r=0.9960. From the slope of the regressive equation, we can found that 32 mV/pH is much smaller than that of 59 mV/pH (which is accordance with one proton and one electron reaction), indicating that there are Redox Bohr effect at the direct electron transfer process [21-23].

3.5 Effect of scan rate

Table 1. Comparison of different biosensor made of Hb and nanomaterials

Conformation of biosensor	Formal potential and peak separation	Linear range	Detection limit	Heterogeneous rate constant, Micheal-Menten Constant	Ref.
Ag@C HRP		5×10^{-7}-1.4×10^{-4}	2.0×10^{-7}	37.5 μM	10
CdSe@CdS GOx	-0.459V vs Ag/AgCl 58 mV	1.6×10^{-4}-5.6×10^{-3}	2.5×10^{-5}	1.56 s^{-1}	11
MCNTs-Au@Au$_2$S$_2$O$_3$-Hb	0.024 V, 91 mV	4×10^{-5}-7.2×10^{-4} M	3.2×10^{-6} M	1.30 s^{-1}, 0.014 mM	12
[Hb/Fe$_3$O$_4$@Pt]$_n$	77 mV	0.125μM-0.16mM(H$_2$O$_2$) 1.5μM-0.12mM(NO$_2^-$)		2.90 s^{-1}	13
Au@Ag NRs-GOD	-0.35 V vs, Ag-AgCl	0.02-7.02 mM (Glucose)	0.67μM		14
(heme protein–Au–PDA–Fe$_3$O$_4$ MBNPs	-381 mV vs SCE	0.75-121.5 μM	0.23μM	3.1 s^{-1} 82.5 μM	18
CNTs-MnO$_2$ nanowires-Hb	-0.339V, 58 mV	1.0×10^{-7}~2.0×10^{-4} M	2.4×10^{-8} M	1.10 s^{-1}, 0.32 mM	25
MCNTs-Ag NPs-Mb	-0.295 V, 160 mV	2×10^{-6}-1.2×10^{-3}M	3.6×10^{-7} M	0.41 s^{-1}, 1.62 mM	26
Electrodeposited CS-MCNTs-Au NPs-Hb	-0.289 V, 100 mV	1×10^{-6}-4.7×10^{-4} M	5.0×10^{-7} M	0.74 s^{-1}, 1.61 mM	27
hexagonal mesoporous silica/Hb	-0.037 V and -0.232 V; 104 mV	0.4-6.0 μM(H$_2$O$_2$) 0.2-3.8 μM(NO$_2^-$)	1.86×10^{-9} M 6.11×10^{-7}M	0.92 ± 0.18 s^{-1}, 12.3 ± 0.84 μM	28
NGR-CdS@TiO$_2$-Hb	-0.395 V, 50 mV	1.0×10^{-7}-6.8×10^{-5} M	5.4×10^{-8} M	3.60 s^{-1}, 0.012 mM	This work

The effect of scan rate on the direct electron transfer behavior of Hb entrapped in NGR-CdS@TiO$_2$ composite film has also been investigated. The typical cyclic voltammograms of NGR-CdS@TiO$_2$-Hb/Au in pH 7 PBS at the scan rate from 10 to 300 mV/s is shown in Fig.5. It is found that the peak current is linear to the square root of scan rate with regression equations of I_{pa}=-15.36+93.30$v^{1/2}$, r=0.9954; I_{pc}=9.702-86.17$v^{1/2}$, r=0.9982. The excellent linearity and the axial symmetry demonstrate a fast electron transfer and diffusion-controlled process of Hb in the composite

NGR-CdS@TiO_2 film. Further investigation of the relationship of peak potential versus scan rate, it is found that the peak separation keeps almost unchanged in low scan rate (10 to 80 mV/s), and peak potential is linear to the natural logarithm of scan rate with regression equation of E_{pa}=-0.2722+0.03908ln$v$, r=0.9733; E_{pc}=0.5208-0.04088ln$v$, r=0.9850 (v>100 mV/s). Based on Laviron equation [24],

$$E_{pa} = E^{o'} + \frac{RT}{\alpha nF} \ln \frac{\alpha nF k_s}{RT} + \frac{RT}{\alpha nF} \ln v$$

$$E_{pc} = E^{o'} - \frac{RT}{(1-\alpha)nF} \ln \frac{(1-\alpha)nFK_s}{RT} - \frac{RT}{(1-\alpha)nF} \ln v$$

$$\log k_s = \alpha \log(1-\alpha) + (1-\alpha)\log \alpha - \log(RT/nFv) - \alpha(1-\alpha)nF\Delta E_p/2.3RT$$

In the upper equations, α is the electron transfer coefficient, n is the electron transfer number, k_s is the apparent heterogeneous electron transfer rate constant (s^{-1}), v is the scan rate (V/s). Experimental results showed that the scan rate in the range of 10-500 mV/s did not affect the k_s value. Assuming α=0.5 and v=0.3 V/s, the heterogeneous electron transfer rate can be calculated to be 3.60 s^{-1}. The calculated value is much larger than those reports for Hb immobilized on CNTs-MnO_2 nanowires (1.10 s^{-1}) [25], Ag NPs doped CNTs modified gold electrode (0.41 s^{-1}) [26], electrodeposited CS-MCNTs-Au NPs-Hb (0.74 s^{-1}) [27] and core/shell Au@$Au_2S_2O_3$-CNTs (1.3 s^{-1}) [12]. The detail comparison of biosensors modified with different nanomaterials can be seen in Table 1. The easy, fast and stable electron transfer of Hb in NGR-CdS@TiO_2 can serve as an efficient biosensor.
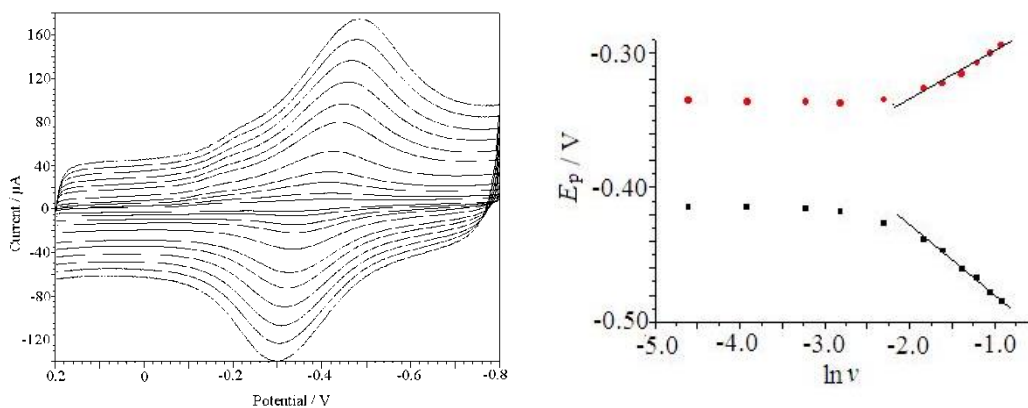

Figure 5. CVs of NGR-CdS@TiO_2-Hb/Au in pH 7 PBS under various scan rates.

3.6 Electrocatalysis towards oxygen

In deoxygenated pH 7 PBS, NGR-CdS@TiO_2-Hb/Au shows only one pair of redox peaks in the potential range of 0.2 V to -0.8 V. When being bubbled a volume of air into the cell containing pH 7 PBS, the reduction peak increases and oxidation peak decreases. Fig.6 shows the CVs of NGR-CdS@TiO_2-Hb/Au under different deoxygenated time. It is found that the reduction peak current decrease and oxidation peak current increase with deoxygenated time increasing, and the CVs will maintain unchanged up to 20 min, so in the latter experiments, the direct electron transfer investigation can be carried out after 20 min deoxygenation by high purity of N_2. The electrocatalytic response

towards oxygen is the traditional feature of electro-catalytic current. According to the reference [29], the possible catalytic mechanism can be deduced to be below:
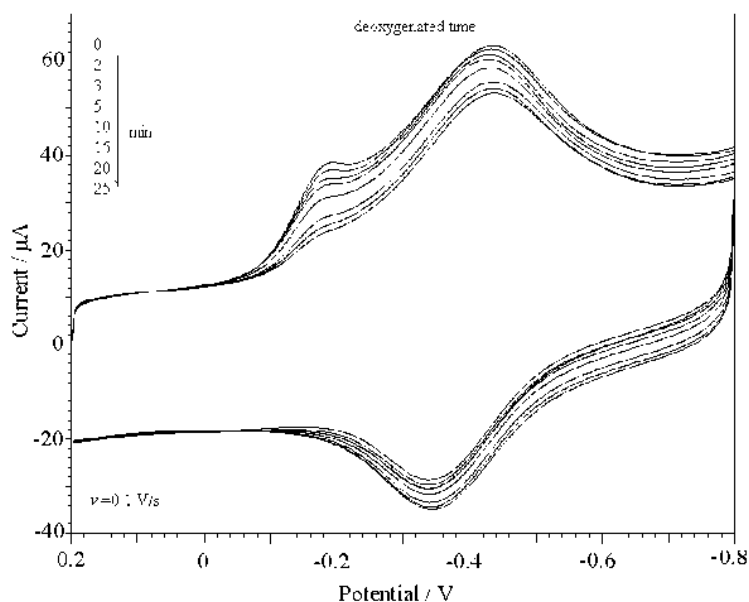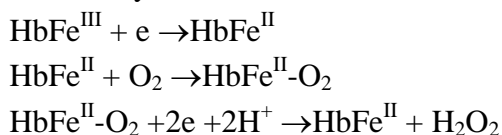
$$HbFe^{III} + e \rightarrow HbFe^{II}$$
$$HbFe^{II} + O_2 \rightarrow HbFe^{II}\text{-}O_2$$
$$HbFe^{II}\text{-}O_2 + 2e + 2H^+ \rightarrow HbFe^{II} + H_2O_2$$

Figure 6. Electrocatalytic behavior of NGR-CdS@TiO$_2$-Hb/Au upon oxygen under different deoxygenated time

3.7 Electrocatalysis towards hydrogen peroxide

The electrocatalytic reduction of hydrogen peroxide at NGR-CdS@TiO$_2$-Hb/Au was also studied by cyclic voltammetry and amperometry. With a stepwise increase of H$_2$O$_2$ concentration in PBS, a stepwise growth of reduction current was observed. Fig.7 is the CVs and i-t curves of NGR-CdS@TiO$_2$-Hb/Au upon successively addition of H$_2$O$_2$ in pH 7 deoxygenated PBS. As seen from the Fig. 7, the reduction peak currents increase with addition of H$_2$O$_2$, the reduction peak potential is about -0.3 V, and when the H$_2$O$_2$ concentration reaches a certain concentration, the reduction peak current increases very slowly. The phenomenon indicates that Hb entrapped in NGR-CdS@TiO$_2$ composite film shows a feature of enzyme-catalytic reaction. From the steady-state amperometric i-t curve, the catalytic current is linear to the concentration of H$_2$O$_2$ from 1.0×10^{-7} to 6.8×10^{-5} mol/L, the regression equation is i (μA)$=0.5286 +3.4255c$ (μmol/L), r$=0.9982$, the detection limit can be calculated to be 5.4×10^{-8} mol/L. As compared to the NGR-Hb mono-modified Au, it is obvious that the stepwise of NGR-Hb/Au is much smaller than that of NGR-CdS@TiO$_2$-Hb/Au, indicating that core/shell CdS@TiO$_2$ nanoparticles can effectively enhance the direct electron transfer of Hb, this phenomenon maybe the biocompatible function of CdS@TiO$_2$ nanoparticles which lead the secondary structure of Hb to be maintained effectively and enhance the DET of Hb in the nanocomposite film. When the addition concentration of H$_2$O$_2$ is larger than 1×10^{-4} mol/L, a current platform can be observed, this is

the typical characteristics of Michealis-Menten enzyme-catalytic dynamics [30]. The Michaelis-Menten constant ($K_m{}^{app}$) can give an indication of the enzyme-substrate kinetics. Based on the Linweaver-Burk equation, the Michealis-Menten constant can be calculated according to the slope and intercept of the regression equation.

$$1/I_{cat} = 1/I_{max} + K_m{}^{app}/I_{max}c$$

Here I_{max} is the maximum current under saturated substrate condition, c is the bulk concentration of H_2O_2, I_{cat} is the steady state current after the addition of substrate, $K_m{}^{app}$ is the Michealis-Menten constant. According to the slope and intercept of the above equation, $K_m{}^{app}$ can be calculated to be 0.012 mM. The value is much smaller than Mb immobilized in CNTs-Ag NPs composite (1.62 mM)[26] and hexagonal mesoporous silica/Hb (0.92 mM) [28], and similar to Au@Au$_2$S$_2$O$_3$-CNTs film (0.014 mM)[12]. The smaller value of $K_m{}^{app}$ of biosensors suggests that Hb entrapped in NGR-CdS@TiO$_2$ composite film has better affinity towards H_2O_2, which can be derived from the favorable micro-environment for the stability and better electron transfer function of Hb in this composite film.
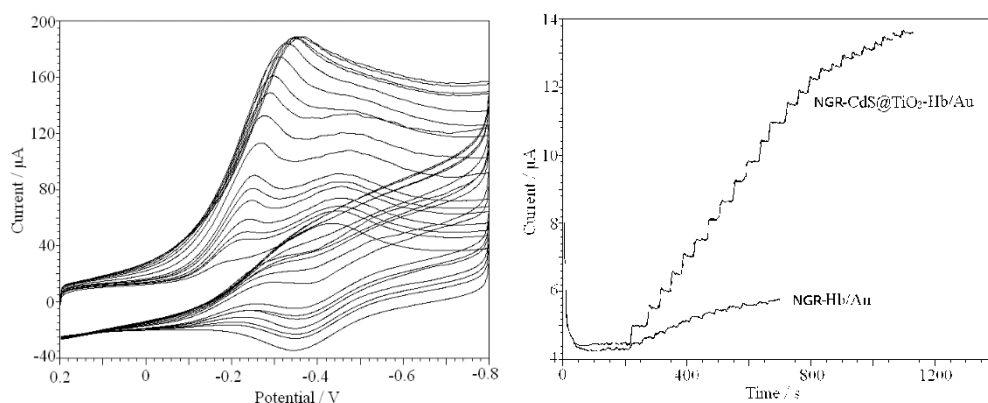

Figure 7. CVs and i-t curve of NGR-CdS@TiO$_2$-Hb/Au upon successive addition of H_2O_2.

3.8 Stability, reproducibility and interference

The stability and reproducibility of the proposed electrode have also been investigated. After modification of the proposed electrode, it was stored in 4°C refrigerator and pH 7 PBS for three week, the biosensor retained 92.3% of its original current response. The same modified electrode was used to successive cyclic voltammetric measurements for 11 times respectively, the relative standard derivation is 3.4% and 4.5% to 2.5 μM H_2O_2. The results suggest that the biosensor has favorable stability and reproducibility.

The interference of other substances to the determination of H_2O_2 has also been studied. The results shows the common interferents such as dopamine, ascorbic acid, uric acid, glucose, acetaminophen and amino acids have no obvious interference to the determination of H_2O_2, however, the addition of 10 times of hydroquinone will produce obvious promotion of catalytic current of H_2O_2. The results also prove that the biosensor can be utilized for practical application in simulated and real samples.

3.9. Sample analysis

As the proposed biosensor shows favourable stability and reproducibility, the simulated and real samples have been used for evaluation of the precision. The content of H_2O_2 in real and simulated samples were determined by the standard fluorescence method to compare with determined value by this proposed method. The simulated sample was prepared by addition of different content of H_2O_2 into real urine, and the real sample was prepared from the attenuation of medical hydrogen peroxide and 84 liquid disinfectant ® with pH 7 PBS to a suitable concentration, the proposed biosensor was utilized to determine the concentration of H_2O_2 and the recoveries. The recoveries for the simulated and real samples are 94.3-103.4% and 91.8-105.2%, respectively (Table 2). All the results indicate that the proposed methodology has favourable accuracy and can be used to determine H_2O_2 in practical application.

Table 2. Determination of H_2O_2 in real and simulated samples

Sample	Added / μM	Detn. by standard method / μM	Detn. By this method / μM	Recovery / %
PBS+standard solution	10.0	9.94	9.95	99.5
Urine+PBS+standard solution	10.0	9.94	9.43	94.3
Simulated sample by adding some interfering substances+PBS	10.0	9.91	103.4	103.4
Real samples(84 liquid disinfectant)	10.0	9.46	9.18	91.8
Real samples(84 liquid disinfectant+some interfering substance)	10.0	10.03	10.52	105.2

4. CONCLUSION

NGR and core/shell $CdS@TiO_2$ nanoparticles were prepared and used for direct electrochemistry investigation of Hb and hydrogen peroxide biosensor fabrication. Direct electron transfer and electrocatalytic activities of Hb were investigated. The results demonstrated that the quasi-reversible and reproducible cyclic voltammetry of direct electron transfer of Fe center in Hb with formal potential of -0.395 V and fast heterogeneous rate constant of 3.60 s^{-1}was realized on NGR-CdS@TiO$_2$ modified Au. The proposed biosensor showed advantages in stability, reproducibility, low detection limit of 5.4×10^{-8} mol/L, low Michealis-Menten constant (0.012 mM) and favorable recoveries of 94.3-103.4% and 91.8-105.2% for simulated and real samples, and the proposed biosensor has a potential application for the determination of hydrogen peroxide.

CONFLICTS OF INTEREST
There are no conflicts to declare.

References

1. Y. H. Wu and S.S. Hu, *Microchim. Acta*, 159(2007)1.
2. F. Chekin, J. B. Raoof, S. Bagheric, S. B. Abd Hamid, *Anal. Methods*, 4(2012)2977.
3. N. Lavanya, S. Radhakrishnan, C. Sekar, *Biosens. Bioelectron.*, 36(2012)41.
4. Y. Zeng, W. Li, H.H. Zhang, X. Wu, W. Sun, Z.H. Zhu, Y. Yu, *Anal. Methods*, 6(2014)404.
5. C. Yu, H. Sun, S.F. Hou, *Anal. Methods*, 9(2017)4873.
6. M. Zhang, Z.Z. Huang, G.Y. Zhou, L. Zhu, Y. Feng,T. Lin, H. Q. Hou, Q.H. Guo, *Anal. Methods*, 7(2015)8439.
7. K. Vijayaraj , S. W. Hong, S.-H. Jin, S-C Changc, D.-S. Park, *Anal. Methods*, 8(2016)6974.
8. Q. Huasin, *Anal. Methods*, 9(2017)6734.
9. C.L. Pan, B. Hu, W. Li, Y. Sun, H. Ye, X.X. Zeng, *J. molec. Cata.: B Enzy.*, 61(2009)208
10. S.X. Mao, Y.M. Long, W.F. Li, Y.F. Tu, A.P. Deng, *Biosens. Bioelectron.*, 48(2013)258.
11. F.Y. Huang, F. Wang, S.Q. Feng, Y.J. Li, S.X. Li, Y.C. Li, *J. Solid state Electrochem.*, 17(2013)1295.
12. Y.J. Li, F.Y. Huang,Z.X. Luo, B. Xu, X.X. Wang, F.M. Li, F. Wang, L.H. Huang, S.X. Li, Y.C. Li, *Electrochim. Acta*, 74(2012)280.
13. C.M. Yu, Y.D. Wang, L. Wang, Z.K. Zhu, N. Bao, HY Gu, *Coll. Surf. B: Biointerfaces*, 103(2013)231.
14. X.J. Yang, Y.H. Wang, Y.W. Liu, X. Jiang, *Electrochim. Acta*, 108(2013)39.
15. S.H. Liu, F. Lu, Y. Liu, L.P. Jiang, J.J. Zhu, *J. Nanopart. Res.*, 15(2013)1331.
16. H.P. Peng, R.P. Liang, J.D. Qiu, *Biosens. Bioelectron.*, 26(2011)3005.
17. Y. Liu, T. Han, C. Chen, N. Bao, C.M. Yu and H.Y. Gu, Electrochim. Acta, 2011, 56, 3238.
18. H.P. Peng, R.P. Liang, L. Zhang, J.D. Qiu, *J. Electroanal. Chem.*, 700(2013)70.
19. D. Long, W. Li, L. Ling, J. Miyawaki, I. Mochida, S.-H. Yoon, *Langmuir*, 26(2010)16096.
20. Z.H. Chi, S.A. Asher, *Biochemistry,* 37(1998)2865.
21. J.M. Xu, W. Li, Q.F. Yin, H. Zhong, Y.L. Zhu, L.T. Jin, *J. Colloid. Interface Sci.*, 315(2007)17.
22. W. J. Ouart. *Rev. Biophys.*, 1(1968)35.
23. A.M. Bond, Modern Polarographic Methods in Analytical Chemistry, Marcei Dekker, New York, 1980: 27
24. E. Laviron, *J. Electroanal. Chem.,* 101(1979)19.
25. C.Y. Liu, E.Y. Shi, J.P. Yao, R. Peng, *Int. J. Electrochem. Sci.*, 13(2018)5253.
26. C.Y. Liu, J.M. Hu, *Biosen.Bioelectron.*, 24(2009)2149.
27. C.Y. Liu, J.M. Hu, *Electroanal.*, 20(2008)1067.
28. Z.H. Dai, S.Q. Liu, H.X. Ju, H.Y. Chen, *Biosens. Bioelectron.*, 19(2004)861.
29. A. C. Onuoha, X. Zu, J. F. Rusiing, *J. Am. Chem. Soc.*, 119(1997)3979.
30. R.A. Kamin, G.S. Willson, *Anal. Chem.*, 52(1980)1198.